NRIAG JOURNAL OF ASTRONOMY AND GEOPHYSICS
2025, VOL. 14, NO. 1, 71–79
https://doi.org/10.1080/20909977.2025.2456354

Evaluating the photometric performance of KFISP: a comparative analysis with standard catalogs

H. I. Abdel Rahman, I. Zead and R. M. Samir

Astronomy Deptartment, National Research Institute of Astronomy and Geophysics (NRIAG), Cairo, Egypt

ABSTRACT
The Kottamia Faint Imaging Spectro-Polarimeter (KFISP) was recently designed for installation on the 1.88 m Cassegrain Telescope at the Kottamia Astronomical Observatory (KAO) in Egypt. A retrofit was implemented to address optical issues in the initial design of KFISP. This paper presents a comparison of photometric standard magnitudes for the open star cluster M52 and two published catalogues of standard stars, using KFISP in BV filters. For this comparison, a number of statistical tools were used, such as analysis of variance (ANOVA), statistical hypothesis testing, and correlation coefficients. For BV filters, the correlation coefficients between the published catalogues and KFISP observations are remarkably strong. ANOVA results show no significant differences in standard magnitudes between KFISP and the other sources for both standard stars and the M52 open star cluster, demonstrating that KFISP observations are consistent with the published catalogues.

ARTICLE HISTORY
Received 23 July 2024
Revised 28 December 2024
Accepted 12 January 2025

KEYWORDS
Correlation coefficients and ANOVA; KFISP; standard magnitudes; standard stars and star cluster M52

1. Introduction

The Kottamia Faint Imaging Spectro-Polarimeter (KFISP) was recently developed and designed for installation on the Cassegrain Focus of the 1.88 m diameter telescope at the Kottamia Astronomical Observatory (KAO), Egypt. The optical design of KFISP supports various operational modes, including direct imaging, spectroscopy, polarimetric imaging, and spectropolarimetry. To meet polarimetric requirements, KFISP employs an all-refractive design and features a focal reducer with a corrector section, collimator section, parallel beam section (containing various imaging components), and camera section. The corrector section provides an unvignetted Field-of-View (FoV) of $8' \times 8'$, while the collimator section, with a focal length of 305 mm, matches the focal ratio of the input beam. The parallel beam section is 200 mm long and houses the image of the telescope pupil near its midpoint. The camera section, comprising five elements, has a focal length of 154.51 mm, resulting in an effective final focal ratio of f/6.14 (acting as a telescope focal reducer with a 1:2 ratio).

KFISP includes an internal calibration system with a calibration light injection system and an integrating sphere equipped with necessary calibration light sources. The opto-mechanical components of KFISP consist of a double-layered carbon fibre strut structure, and subsystems such as slit and guider assemblies, filter wheel drawer, grism wheel drawer, polarimetric components cubical box, and a CCD (charged couple device) camera integrated with camera optics. The CCD camera features a 2048×2048 pixel array with 13.5-micron square pixels, cooled by liquid nitrogen and fixed to KFISP through the integrated camera lens. KFISP has been fully commissioned and installed. It is currently undergoing tests in all operating modes to confirm its scientific objectives, optical settings, opto-mechanical implementation, and instrumental performance (Azzam et al. 2021).

Several errors in the initial design of the focal reducer were discovered which an oversight of the optical designer were. Those were related to the guide field which was found to be severely limited or completely non-functional and was limiting the versatility of the KFISP. In addition, the triplet encircled energy of that focal reducer was found to degrade the performance of the telescope and contribute to the observed image fall-off at the KFISP imaging plane and did not deliver diffraction-limited performance at the slit plane.

As a result, a new focal reducer was designed such that it has four elements and a much larger diameter to accommodate the off-axis guider field. The quadruplet design, with one extra glass element, has significantly improved the optical performance and allowed the encircled energy to be dramatically improved. Also, the wavefront error was dramatically improved and is very close to diffraction-limited except in the blue. However, it was found that there is still a fall-off in

CONTACT H. I. Abdel Rahman helal_ismaeil@yahoo.com Astronomy Department, National Research Institute of Astronomy and Geophysics (NRIAG), Helwan, Cairo 11421, Egypt

relative intensity of about 7% at the corner of the detector, which is inherent in the design of the telescope.

A retrofit was implemented to correct optical problems in the initial design of KFISP. Hendy and Abdel Rahman (2022) verified the KFISP observations on extended objects through statistical comparisons in the BV bands. They used the open star cluster M67 as an example, demonstrating that there were no significant differences between the published catalogues and Kottamia observations.

The purpose of this paper is to evaluate the quality of the point source observations (individual stars) from the KFISP in light of the recent modifications, and to further confirm the accuracy of results obtained by Hendy and Abdel Rahman (2022) by observing another example of star cluster. By using BV band observations from KFISP, we compare standard magnitudes for standard stars and the open cluster M52 with those from earlier studies. Although the BV filters were chosen for this investigation, the results could be applied to the remaining Johnson-Kron-Cousins broadband (e.g. UBVRI). Statistical comparisons between our observations and available data from literature are employed to evaluate the quality and deviations from published results, ensuring the reliability of KFISP in photometric observations. Observations and data reduction are presented in Section 2, statistical comparison methods are illustrated in Section 3. Results and discussions of BV magnitudes compared to published photometric data are shown in Section 4. Finally, conclusions are presented in Section 5.

2. Observations and data reductions

The photometric observations for this study were conducted using KFISP. Our focus was primarily on the well-known standard fields introduced by Landolt (2013). These fields include SA 41, SA 23, GD 277, GD 278, GD 279, GD 391, GD 405, GD 421, GD 8, GD 10, GD 2, GD 275, and PG2213–006. These fields provide an internally consistent and homogeneous list of standard stars in the Johnson-Kron-Cousins broadband UBVRI photometric system. Published by Landolt (2013), this system has facilitated the standardisation of broadband photometric data for most telescopes, with the stars' locations near the celestial equator making them accessible to telescopes in both hemispheres. A detailed history of this photometric system is available in Landolt (2013). The field of view for these standard stars is depicted in Figure 1.

These standard stars and the open cluster M52 were observed over three nights, from October 16 to 18, 2023, using B and V filters, as detailed in Tables 1 and 2. The observations were compared with data from three published references: Landolt's (2013) catalogue of faint UBVRI standard star fields, the AAVSO Photometric All-Sky Survey (APASS) DR9 (Henden et al. 2016), and Pandey et al. (2001) catalogue of UBVI photometry for NGC 7654 (M52). Basic reduction of the CCD frames was performed using the IRAF package (the Image Reduction and Analysis Facility).

The IRAF package is utilised to reduce the observed CCD frames, below the description of IRAF different tasks that used to reduce the photometric CCD frames.

Task (1): Zerocombine, Bias (or zero) is an offset that occurs when a pixel is read from the CCD camera. Unfortunately, bias can vary across the image. A bias frame is essentially a zero-length exposure (or as close as possible to zero length) with the shutter closed. Zerocombine, is task for combine and process the zero level of the images, the zero level images in the input image list are combined. In each case, the output pixel data type will be real.

Task (2): Flatcombine, Each pixel in the camera has a slightly different sensitivity to light. These sensitivity differences add another noise component to the image (known as flat-fielding error) unless steps are taken to compensate. Flatcombine, is task for combine and process the flat field images, the flat field images in the input image list are combined. If there is more than one subset (such as more than one filter) then the input flat field images are grouped by subset and combined separately.

Task (3): ccdproc it is for process CCD images. ccdproc processes CCD images to correct and calibrate for detector defects, readout bias, zero level bias, dark counts, response, illumination, and fringing. It is efficient, one has to do is setting the parameters and then begin the processing of calibration images.

The CCD image includes signals from different sources, so in the process of CCD reduction, the calibrated science images that represent signal from the star are obtained. The calibration of scientific images requires a specific type of technical frames; it should be obtained at the same temperature as that of the science frames. Science images should be corrected for Bias, Dark and Flat Field using the following equation:

$$Corrected\ imge = \frac{(Scince\,frame - Bias - Dark)}{(Flat\ Field - Bias - Dark)}$$

To obtain instrumental magnitudes, we utilised the Point Spread Function (PSF) fitting available in the DAOPHOT package (is a package for stellar photometry designed to deal with crowded fields) on IRAF (Stetson 1987; Stetson et al. 1992) and calculated standard magnitudes. The errors of calculated magnitudes are approximately 0.05.

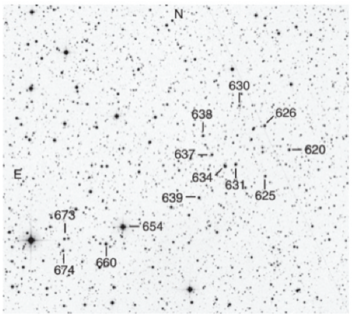

a) The field of view of SA 41

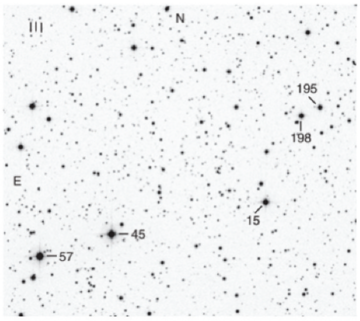

b) The field of view of SA 23

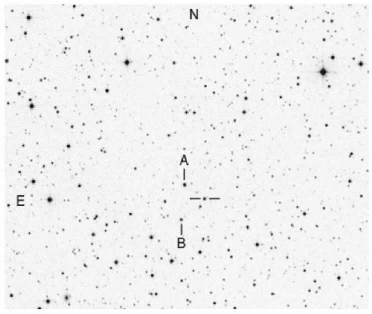

c) The field of view of GD 277

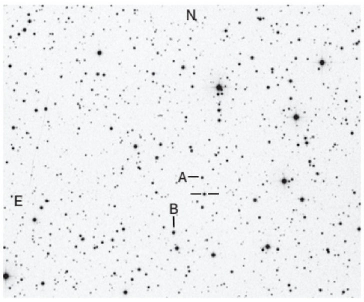

d) The field of view of GD 278

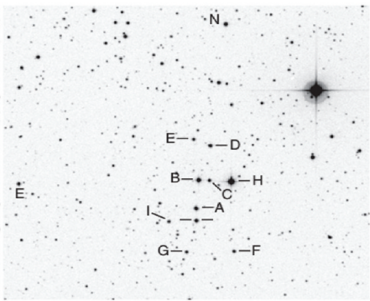

e) The field of view of GD 279

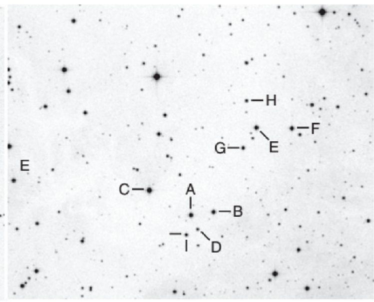

f) The field of view of GD 391

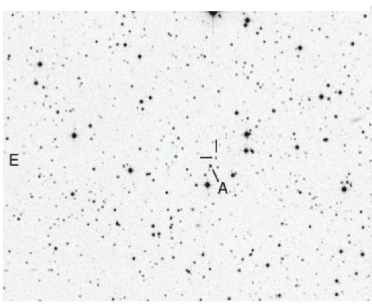

g) The field of view of GD 405

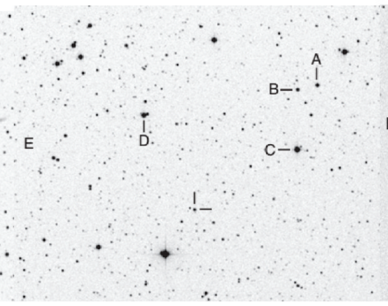

h) The field of view of GD 421

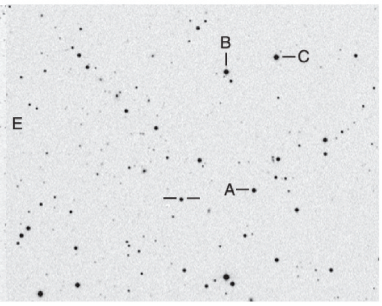

i) The field of view of GD 8

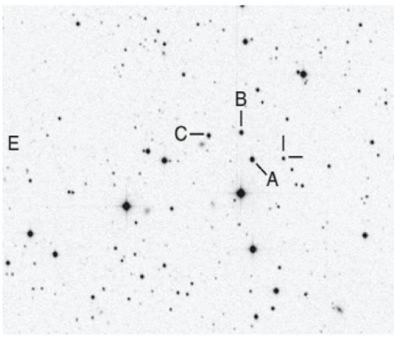

j) The field of view of GD 10

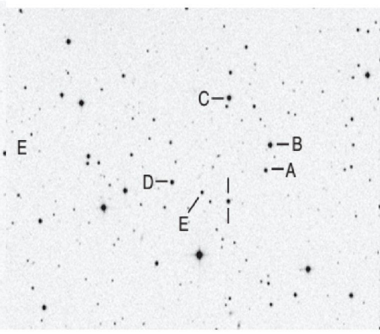

k) The field of view of GD 2

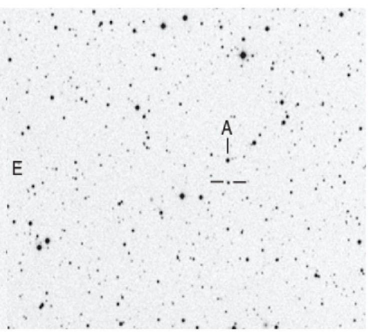

l) The field of view of GD 275

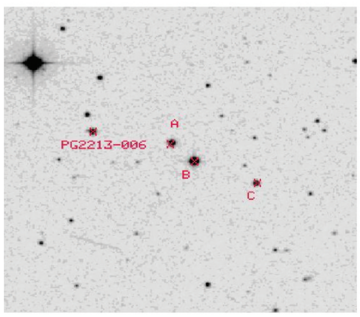

m) The field of view of PG2213-006

Figure 1. The field of view of some standard stars from Landolt (2013) (a,b,c,d,e,f,g,h, i,j,k,l and m).

Table 1. The Kottamia observations by KFISP of some standard stars and two published catalogues. Column (1) shows the object ID. Column (2) and (3) indicate the right ascension and the declination coordinates, respectively. Columns 4, 5 and 6 illustrate the magnitudes in V band from Kottamia observations, Landolt (2013), and Henden et al. (2016), respectively. Columns 7, 8, and 9 present the magnitudes in B band from Kottamia observations, Landolt (2013), and Henden et al. (2016), respectively.

OBJ_ID	ra	Dec	k_V	L_V	H_V	k_B	L_B	H_B
SA 41–634	21 53 27.209	+45 35 40.95	13.184	13.164	13.172	13.923	13.934	13.973
SA 41–631	21 53 24.561	+45 35 45.09	13.339	13.390	13.357	13.629	13.636	13.648
SA 41–639	21 53 33.743	+45 34 20.95	14.130	14.130	14.121	15.450	15.450	15.511
SA 41–638	21 53 32.591	+45 37 00.50	14.167	14.045	14.054	14.838	14.781	14.833
SA 41–637	21 53 30.416	+45 36 11.04	14.461	14.426	14.438	15.641	15.625	15.702
SA41–630	21 53 23.508	+45 38 17.36	15.322	14.986	15.024	16.112	16.025	16.134
SA 41–626	21 53 17.263	+45 37 24.48	14.086	14.058	14.086	14.953	14.969	14.992
SA 41–620	21 53 11.306	+45 36 21.13	14.129	14.176	14.219	14.871	14.946	15.015
SA 23–15	03 44 05.128	+45 06 03.00	10.662	10.658	10.647	11.033	11.033	11.122
SA 23–198	03 43 56.438	+45 09 41.46	11.559	11.559	11.572	11.815	11.751	11.122
SA 23–195	03 43 51.964	+45 10 02.52	12.132	12.125	12.132	12.800	12.813	12.927
GD 277A	01 29 28.971	+51 09 19.49	13.811	13.811	13.856	15.010	15.069	15.172
GD 277B	01 29 29.917	+51 08 02.46	14.519	14.524	14.554	15.175	15.183	15.306
GD 277	01 29 23.992	+51 08 46.99	13.498	13.536	13.576	13.431	13.431	13.546
GD 278B	01 31 06.659	+53 20 17.12	14.348	14.205	14.194	14.898	14.898	14.937
GD 278	01 30 58.075	+53 21 39.40	14.899	14.899	14.818	14.894	15.085	14.994
GD 278A	01 30 58.464	+53 22 17.91	14.998	14.851	14.877	16.300	16.298	16.445
GD 279B	01 52 02.409	+47 01 41.48	11.750	11.714	11.675	12.004	11.981	11.961
GD 279	01 52 02.960	+47 00 06.64	12.457	12.457	12.415	12.544	12.544	11.961
GD 279D	01 51 59.862	+47 03 02.63	13.304	13.241	13.213	13.822	13.799	13.792
GD 279F	01 51 55.046	+46 58 52.28	13.880	13.946	13.896	14.441	14.514	14.476
GD 279C	01 52 00.142	+47 01 40.56	13.945	13.913	13.910	14.942	14.981	14.995
GD 279E	01 52 03.399	+47 03 18.06	14.068	14.011	13.981	14.771	14.747	14.739
GD 279G	01 52 05.094	+46 58 51.38	14.161	14.156	14.118	14.678	14.691	14.710
GD 279A	01 52 02.968	+47 00 34.16	13.455	13.050	13.017	14.077	14.046	14.026
GD 391c	20 30 02.922	+39 15 03.75	11.445	11.463	11.464	12.223	12.223	12.140
GD 391A	20 29 55.304	+39 14 13.08	12.308	12.315	12.316	12.728	12.725	12.713
GD 391B	20 29 51.196	+39 14 20.33	12.888	12.710	12.713	13.489	13.290	13.272
GD 391	20 29 56.177	+39 13 32.19	13.378	13.378	13.380	13.283	13.227	13.210
GD 391G	20 29 45.987	+39 16 34.95	13.619	13.675	13.682	14.913	14.475	14.465
GD 391D	20 29 54.035	+39 13 43.44	14.972	15.012	14.997	15.932	16.006	15.984
GD 405A	23 16 44.966	+47 26 59.90	16.107	15.615		16.809	16.678	
GD 405	23 16 43.875	+47 27 15.57	16.751	16.751		16.585	16.585	
GD 421C	01 50 34.378	+67 41 53.09	12.080	12.158	12.208	14.533	14.533	14.559
GD 421D	01 51 31.415	+67 42 39.05	12.510	12.455	12.473	13.638	13.583	13.604
GD 421	01 51 10.260	+67 39 32.25	14.414	14.414	14.441	15.054	14.201	14.250
GD 8C	00 39 37.145	+31 37 03.40	13.311	13.299	13.319	13.935	13.935	13.995
GD 8B	00 39 44.863	+31 36 36.48	13.687	13.653	13.682	14.490	14.456	14.507
GD 8A	00 39 40.965	+31 32 44.53	14.614	14.593	14.604	15.273	15.288	15.323
GD 8	00 39 52.163	+31 32 29.19	14.699	14.699	14.700	14.507	14.424	14.506
GD 10A	01 06 58.606	+39 30 53.12	13.727	13.694	13.706	14.518	14.518	14.510
GD 10B	01 07 00.369	+39 31 35.07	14.216	14.194	14.180	14.778	14.766	14.705
GD 10C	01 07 05.379	+39 31 28.37	14.413	14.388	14.365	14.942	14.910	14.868
GD 10	01 06 53.995	+39 30 56.92	15.456	15.456	15.487	15.681	15.654	15.560
GD 2B	00 07 25.484	+33 19 00.17	13.286	13.279	13.204	13.867	13.867	13.799
GD 2C	00 07 32.355	+33 20 14.69	13.346	13.314	13.249	13.956	13.933	13.862
GD 2	00 07 32.261	+33 17 27.62	13.802	13.802	13.733	13.615	13.507	13.475
GD 2D	00 07 41.634	+33 17 57.33	14.250	14.255	14.186	14.893	14.860	14.811
GD 2A	00 07 26.174	+33 18 19.18	14.836	14.853	14.789	15.709	15.765	15.663
GD 2E	00 07 36.675	+33 17 41.73	15.189	15.188	15.139	15.789	15.763	15.672
GD 275A	01 18 54.297	+52 27 49.99	15.075	15.019	14.990	16.502	16.502	16.413
GD 275	01 18 54.162	+52 27 13.59	15.683	15.683	15.684	15.890	15.827	16.413
PG2213-006B	22 16 22	−00 21 51	12.740	12.706	12.717		13.455	13.458
PG2213–006	22 16 28	−00 21 17	14.124	14.124	14.128		13.907	13.975
PG2213-006A	22 16 24	−00 21 29	14.215	14.178	14.188		14.851	14.853
PG2213-006C	22 16 18	−00 22 18	15.147	15.109	15.117		15.830	15.879

3. Statistical comparison method

To validate the observations from the Kottamia Telescope using the new KFISP device, we compared our data with two published photometric catalogues of standard stars and two others for the open cluster M52, all in BV filters. The comparison was performed using correlation coefficients and one-way analysis of variance (ANOVA) for the apparent magnitudes of the stars.

First, we examined the correlation coefficient between the observations for each filter, such as B and V. These correlations were calculated using the Pearson correlation coefficient (Bobko 2001) as shown in equation (1):

$$r_{xy} = \frac{\sum_{i=1}^{n} x_i y_i - \sum_{i=1}^{n} x_i \sum_{i=1}^{n} y_i}{\sqrt{n \sum_{i=1}^{n} x_i^2 - \left(\sum_{i=1}^{n} x_i\right)^2} \sqrt{n \sum_{i=1}^{n} y_i^2 - \left(\sum_{i=1}^{n} y_i\right)^2}} \quad (1)$$

r_{xy} = Pearson correlation coefficient between x and y

n = number of observations

x_i = value of x (for i-th observation)

y_i = value of y (for i-th observation)

Table 2. The Kottamia observations by KFISP of M52 and two published catalogs. Column (1) shows the object ID. Column (2) and (3) indicate the right ascension and the declination coordinates, respectively. Column (4) and (5) illustrate the magnitudes from Kottamia observations in B and V bands, respectively. Column (6) and (7) refer to magnitudes from Simbad in B and V bands, respectively. Column (8) and (9) show magnitudes from Pandey et al. (2001) data in B and V bands, respectively.

OBJ_ID	Ra	Dec	K_B	K_V	S_B	S_V	P_B	P_V
NGC 7654 1082	23 25 25.26591	+61 35 34.5899	13.309	12.802	13.360	12.830	13.369	12.891
NGC 7654 1062	23 25 21.06752	+61 32 35.8148	12.790	12.290	12.050	12.290	12.867	12.381
NGC 7654 1042	23 25 15.03507	+61 38 33.8316	13.424	13.048	13.424	12.988	13.464	13.024
NGC 7654 1007	23 25 06.79371	+61 34 29.3472	13.940	13.389	14.020	13.480	14.025	13.478
NGC 7654 1005	23 25 06.26536	+61 37 26.2061	14.079	13.548	14.140	13.580	14.224	13.621
NGC 7654 992	23 25 02.10450	+61 33 28.0867	13.918	13.418	14.000	13.460	13.979	13.494
NGC 7654 981	23 24 58.29597	+61 33 26.9577	13.864	13.340	13.980	13.380	14.019	13.447
NGC 7654 980	23 24 58.29675	+61 38 09.9259	14.592	14.001	14.640	13.990	14.698	14.048
NGC 7654 969	23 24 56.33359	+61 33 27.3850	14.680	14.151	14.800	14.180	14.785	14.233
NGC 7654 968	23 24 56.25755	+61 36 38.2368	12.296	11.798	11.990	11.680	12.392	11.872
NGC 7654 964	23 24 55.46323	+61 35 41.1820	14.455	13.867	14.500	13.870	14.538	13.929
NGC 7654 963	23 24 55.11333	+61 34 06.6547	13.907	13.351	13.990	13.380	14.023	13.438
NGC 7654 949	23 24 53.11	+61 35 22.2	14.248	13.721	14.300	13.720	14.326	13.801
NGC 7654 941	23 24 51.86476	+61 31 33.2453	12.265	11.863	12.400	11.940	12.374	11.997
NGC 7654 936	23 24 51.33374	+61 35 14.0651	13.266	12.797	13.350	12.830	13.389	12.894
NGC 7654 929	23 24 49.82903	+61 35 58.5173	13.200	12.805	13.293	12.841	13.292	12.879
NGC 7654 926	23 24 49.35885	+61 37 36.9385	11.538	11.120	11.440	11.100	11.576	11.056
NGC 7654 920	23 24 48.78248	+61 32 12.3508	13.657	13.219	13.770	13.330	13.762	13.335
NGC 7654 919	23 24 48.99848	+61 32 59.6479	14.421	13.915	14.520	13.960	14.517	14.003
NGC 7654 918	23 24 48.79467	+61 34 30.4751	12.093	11.711	12.140	11.730	12.200	11.818
NGC 7654 916	23 24 49.08201	+61 36 44.3988	11.702	11.232	11.460	11.060	11.790	11.219
NGC 7654 910	23 24 47.69541	+61 37 39.0992	12.557	12.108		12.170	12.654	12.163
NGC 7654 902	23 24 45.17848	+61 34 45.9417	14.312	13.850	14.380	13.850	14.414	13.958
NGC 7654 885	23 24 42.26	+61 31 19.4	12.566	12.091	12.690	12.170	12.693	12.240
NGC 7654 884	23 24 42.50416	+61 36 12.7052	12.517	12.131	12.420	12.020	12.676	12.235
NGC 7654 879	23 24 41.90890	+61 32 33.0362	12.781	12.379	12.890	12.430	12.884	12.492
NGC 7654 876	23 24 41.20534	+61 34 10.6004	13.709	13.240	13.840	13.270	13.806	13.292
NGC 7654 868	23 24 39.95453	+61 34 18.2648	13.268	12.864	13.410	12.930	13.428	12.981
NGC 7654 867	23 24 39.77891	+61 37 50.0010	11.318	10.949	11.240	10.810	11.319	10.795
NGC 7654 863	23 24 38.50498	+61 37 17.3532	12.858	12.414		12.480	13.052	12.507
NGC 7654 862	23 24 36.43300	+61 35 16.4963	14.829	14.323	14.850	14.160	14.924	14.335
NGC 7654 858	23 24 37.22	+61 34 56.1	13.925	13.325	14.060	13.350	14.070	13.422
NGC 7654 857	23 24 37.17	+61 38 28.5	14.981	14.434		14.540	15.178	14.545
NGC 7654 852	23 24 35.72965	+61 36 14.0819	14.436	13.943	14.630	14.040	14.653	14.048
NGC 7654 847	23 24 34.32132	+61 33 18.9514	13.570	13.176	13.700	13.250	13.720	13.290
NGC 7654 841	23 24 32.78167	+61 34 42.5198	13.135	12.754	13.310	12.840	13.330	12.870
NGC 7654 840	23 24 33.32165	+61 36 29.3543	14.009	13.541	14.150	13.630	14.179	13.644
NGC 7654 832	23 24 31.17887	+61 32 00.5027	13.900	13.430	14.020	13.510	14.040	13.544
NGC 7654 829	23 24 30.54	+61 37 00.8	13.507	13.024	13.650	13.070	13.709	13.132
NGC 7654 828	23 24 29.79	+61 36 29.4	15.181	14.519	12.520	12.030	15.367	14.614
NGC 7654 821	23 24 28.53052	+61 37 28.6016	13.161	12.684	13.350	12.790	13.443	12.851
NGC 7654 820	23 24 28.54189	+61 38 02.0598	11.636	11.277	11.770	11.360	11.898	11.402
NGC 7654 816	23 24 28.05390	+61 31 53.9209	12.673	12.236	12.770	12.310	12.817	12.381
NGC 7654 815	23 24 27.73274	+61 35 00.7469	12.414	12.073	12.540	12.110	12.607	12.218
NGC 7654 814	23 24 27.20377	+61 32 36.9184	12.825	12.456	12.980	12.590	13.008	12.635
NGC 7654 813	23 24 27.21236	+61 36 47.0903	11.774	11.348	11.970	11.460	12.046	11.480
NGC 7654 810	23 24 25.86470	+61 31 52.1613	13.928	13.342	14.100	13.450	14.092	13.493
NGC 7654 806	23 24 25.09	+61 36 00.6	13.867	13.425	14.030	13.500	14.084	13.548
NGC 7654 798	23 24 23.67416	+61 37 47.2192	13.084	12.622		12.810	13.277	12.721
NGC 7654 785	23 24 21.48874	+61 35 25.9679	14.201	13.759	14.490	13.880	14.465	13.946
Cl* NGC 7654 CKK V6	23 25 10.46115	+61 35 08.6617	15.696	14.916	15.791	14.957	15.755	14.949
Cl* NGC 7654 CKK V5	23 24 37.39226	+61 38 57.8803	14.878	14.298	15.052	14.381	15.130	14.444
Cl* NGC 7654 CKK V4	23 24 45.41677	+61 36 52.0571	17.507	16.375	17.538	16.328	17.450	16.371
Cl* NGC 7654 CKK V25	23 25 16.91005	+61 32 45.6569	16.544	15.691	16.678	15.788	16.557	15.798
Cl* NGC 7654 CKK V23	23 24 40.46043	+61 36 10.5865	16.313	15.562	16.432	15.572	16.325	15.692
Cl* NGC 7654 CKK V2	23 24 35.85820	+61 38 49.8284	12.885	12.499	13.074	12.590	13.139	12.674
Cl* NGC 7654 CKK V11	23 24 49.84641	+61 36 17.0094	12.280	11.896	11.960	11.650	12.249	11.863

Secondly, we applied one-way analysis of variance (ANOVA), a statistical technique used to test whether three or more population means are equal. This method relies on several basic assumptions, the most important of which are:

- **Independence**: The samples must be independent of each other.
- **Normality**: The data in each group should be approximately normally distributed.
- **Homogeneity of variances**: The variances within each group should be roughly equal.

To apply the analysis of variance, it is crucial to verify that the above conditions are satisfied. The verification of these conditions is clarified in the next two sections (3–1 and 3–2, respectively). It should be noted that the first condition, independence of samples, is already satisfied.

3.1. Statistical tests of normality

There are various methods available to test the normality of the data. The most popular methods are the Kolmogorov – Smirnov and Shapiro – Wilk tests.

The statistical hypothesis of the normality is:

The null hypothesis, H_0: The data follow a Normal distribution.

Alternative hypothesis, H_1: The data do not follow a Normal distribution.

The test statistic and the critical regions for Kolmogorov – Smirnov and Shapiro – Wilk tests are explained by (Hendy and Abdel Rahman 2022).

3.2. Test of homogeneity (Levene test for equality of variances)

Homogeneity refers to the equality of variances between groups. Levene's test is utilised to assess the equality of variances for a variable across two or more groups Levene et al. (1960). It tests the null hypothesis (H_0) that the population variances are equal, a condition known as homogeneity. If the resulting p-value of Levene's test is less than a predefined significance level (typically set at 0.05), the null hypothesis of equal variances is rejected. This indicates that there is a sufficient evidence to suggest a difference between the variances in the populations being compared.

3.2.1. The statistical homogeneity hypothesis

$$H_0 : \sigma_1^2 = \sigma_2^2 = \ldots = \sigma_n^2$$

$H_1 : \sigma_i^2 \neq \sigma_j^2$ for at least one pair (i,j).

Also, the test statistic (Levene's test) and the critical region are described by (Hendy and Abdel Rahman 2022).

3.3. Comparison method: analysis of variance (ANOVA)

After confirming the validity of the data test and that it follows the normal distribution and homogeneity test, we can compare the population means using the analysis of variance method.

Analysis of variance (ANOVA) is a set of statistical models used to analyse the differences between means Howell (2002).

- **The statistical hypothesis of ANOVA**

$$H_0 : \mu_1 = \mu_2 = \ldots = \mu_n$$

H_1 :At least two are different.

3.3.1. Test statistic

F test assumes that the observations are normally distributed with a common variance but different means. The formula for the one-way analysis of variance (ANOVA) F-test is

$$F_{calculated} = \frac{MSB}{MSE} \tag{2}$$

$$F_{Tabulated} = F_{k-1,N-k} \tag{3}$$

Where

$$MSB = \frac{1}{k-1} \sum_{i=1}^{k} n_i \left(\bar{Y}_i - \bar{Y}\right)^2 \tag{4}$$

$$MSE = \frac{1}{N-k} \sum_{i=1}^{k} n_i \left(Y_{ij} - \bar{Y}_i\right)^2 \tag{5}$$

MSB and MSE are called the mean square between groups and mean square error.

And

$$\bar{Y} = \frac{1}{N} \sum\nolimits_{i=1}^{k} \sum\nolimits_{j=1}^{n_i} Y_{ij} \tag{6}$$

$$N = \sum_{i=1}^{k} n_i \tag{7}$$

$$\bar{Y} = \frac{1}{n_i} \sum\nolimits_{j=1}^{n_i} Y_{ij} \tag{8}$$

ANOVA calculations are conveniently displayed in the tabular form shown below, which is known as an ANOVA table.

ANOVA Table

Source	Sum of Squares (SS)	df	Mean Square (MS)	F_{obs}	P-value
Treatments	SST	K – 1	MST	(MST/MSE)	$P[F \geq F_{obs}]$
Errors	SSE	*N* - k	MSE		
Total	SSTOT	N –1			

Where:

k is the number of factor levels (treatments) or populations.

y_{ij} is the jth observation in the ith sample, j = 1, . . . , n_i and n_i is sample size for the ith sample.

Df is the degrees of freedom.

3.3.2. The decision

The $F_{Calculated}$ is compared to $F_{Tabulated}$ with K-1 numerator degrees of freedom and N-K denominator degrees of freedom. We can reject H_0 if $F_{Calculated}$ is greater than $F_{Tabulated}$.

Another criterion for accepting or rejecting the null hypothesis, commonly used in statistical programs, is the probability value (p-value) instead of the test statistic. The p-value represents the probability of obtaining results at least as extreme as those observed during the experiment, assuming the null hypothesis is true. If the p-value is smaller than the significance level ($\alpha = 0.05$), we reject the null hypothesis.

4. Results and discussions

4.1. The correlation coefficients (r)

Tables 3 and 4 present Pearson's linear correlation coefficients between observations from Kottamia (KFISP) and the two published catalogues for BV filters regarding standard stars and M52. These coefficients were computed using equation (1) and indicate a very strong correlation, suggesting no significant differences between the observations in these filters. However, while strong correlation provides valuable insight, it alone is insufficient for a comprehensive comparison of Kottamia's observations with those of other authors. The next important step in verifying this comparison is to test the hypothesis.

4.2. Test of normality

The initial step in applying the one-way analysis of variance (ANOVA) method is to test for normality within each of the three populations under examination. Tables 5 and 6 present the results of the normality tests conducted for BV filters comparing KFISP Kottamia with the other datasets.

Tables 5 and 6 show that all p-values in columns 2 and 3 are greater than the significance level ($\alpha = 0.05$). Therefore, we cannot reject the null hypothesis (H_0) that the three populations follow a normal (Gaussian) distribution.

4.3. Test of homogeneity

The second condition is the homogeneity test, which assesses the equality of variances among the three populations. Tables 7 and 8 indicate that the p-values for all three filters are greater than 0.05. Therefore, we can not reject the null hypothesis that the variances are equal across these populations.

After confirming the conditions for applying the analysis of variance test, we applied equations (2 and 3) to test the differences between means for BV filters in the three populations of standard stars and M52. Tables 9–12 present the results of these tests for each filter.

Table 9 compares B filters for standard stars and consists of 6 columns: Column 1 lists the Source of variation for B filters (between groups, within groups (Errors), and total). Column 2 displays the Sum of Squares, and column 3 shows the degrees of freedom. Column 4 presents the Mean Square,

Table 3. The correlation coefficients (r) between Kottamia's KFISP observations and others for standard stars.

Correlation coefficients (r)	B_L	B_H	V_L	V_H
V_K	–	–	99.6%	99.7%
B_K	99.4%	98.7%	–	–

Table 4. The correlation coefficients (r) between Kottamia's KFISP observations and others for M52.

Correlation coefficients (r)	B_S	B_P	V_S	V_P
V_K	–	–	95.5%	99.9%
B_K	95.1%	99.8%	–	–

Table 5. Test of normality of BV filters for standard stars.

Filters	p-value (Kolmogorov-Smirnov)	p-value (Shapiro-Wilk)
B_K	0.066	0.193
B_L	0.200	0.163
B_H	0.052	0.051
V_K	0.200	0.613
V_L	0.153	0.082
V_H	0.153	0.082

Table 6. Test of normality of BV filters for M52.

Filters	p-value (Kolmogorov-Smirnov)	p-value (Shapiro-Wilk)
B_K	0.200	.116
B_S	0.200	.095
B_P	0.200	.343
V_K	0.200	0.381
V_S	0.200	0.389
V_P	0.200	0.617

Table 7. Levene's test for equality of variances for standard stars.

Filters	p-value (Levene Statistic)
All B-Filters	0.999
All V-Filters	0.898

Table 8. Levene's test for equality of variances for M52.

Filters	p-value (Levene Statistic)
All B-Filters	0.934
All V-Filters	0.999

column 5 shows the test statistic (F), and column 6 displays the p-value. Tables 10–12 have similar headings to Table 9.

The results in Tables 9–12 indicate p-values of 0.892, 0.780, 0.849, and 0.877 for BV filters, respectively, which are all greater than the significance level (0.05). Therefore, we can not reject the null hypothesis (H_0) across all filters. This suggests that there are no significant differences between the means of the three populations or observations in B and V filters.

In conclusion, based on this comparison, we find that the observations from KFISP agree with those from the published catalogues for both standard stars and the star cluster M52.

5. Conclusions

The aim of this study is to validate the accuracy of photometric standard magnitudes obtained using KFISP by comparing them with catalogues of standard stars (as point sources) and the open cluster M52 (as an extended object). Strong correlation coefficients have been found between our observations and those from other catalogues in BV bands for both standard stars and M52.

To facilitate this comparison using the analysis of variance (ANOVA) test, it was crucial to verify the conditions for ANOVA application, including normality and homogeneity tests across the three populations in B and V filters for Kottamia observations and published catalogues. Results show that all populations follow a normal (Gaussian) distribution and exhibit homogeneous variances.

The ANOVA comparisons across the three populations in both filters revealed no significant differences between observations for standard stars and M52. This indicates that the photometric measurements obtained by KFISP are consistent with those from other telescopes, thereby affirming the accuracy of the findings previously reported by Hendy and Abdel Rahman (2022).

Table 9. ANOVA of B filters for standard stars.

Source of Variation for B Filters	The sum of Squares SS	Df	Mean Square MS	F (calculated)	P-value
Between Groups	0.361	2	0.180	0.114	0.892
Within Groups (Errors)	251.749	159	1.583		
Total	252.109	161			

Table 10. ANOVA of V filters for standard stars.

Source of Variation for V Filters	The sum of Squares SS	Df	Mean Square MS	F (calculated)	P-value
Between Groups	0.629	2	0.314	0.249	0.780
Within Groups (Errors)	203.262	161	1.262		
Total	203.890	163			

Table 11. ANOVA of B filters for M52.

Source of Variation for B Filters	The sum of Squares SS	Df	Mean Square MS	F (calculated)	P-value
Between Groups	0.523	2	0.262	0.164	0.849
Within Groups (Errors)	262.509	164	1.601		
Total	263.033	166			

Table 12. ANOVA of V filters for M52.

Source of Variation for B Filters	The sum of Squares SS	Df	Mean Square MS	F (calculated)	P-value
Between Groups	0.347	2	0.173	0.132	0.877
Within Groups (Errors)	220.827	168	1.314		
Total	221.174	170			

Disclosure statement

No potential conflict of interest was reported by the author(s).

References

Azzam YA, Elnagahy FIY, Ali GB, Essam A, Saad S, Hamed Ismail IZ, Ahmed NM, Yoshida M, Kawabata KS, Hiroshi Akitaya AS, et al. 2021. Kottamia faint imaging spectro-polarimeter (KFISP): opto-mechanical design, software control and performance analysis. Exp Astron. 53(1):45–70. doi: 10.1007/s10686-021-09802-z.

Bobko P. 2001. Correlation and regression: applications for industrial organizational psychology and management. 2nd ed. Thousand Oaks (CA): Sage Publications.

Henden AA, Templeton M, Terrell D, Smith TC, Levine S, Welch D. 2016. Vizier online data catalog: AAVSO photometric all sky survey (APASS) DR9. yCat,2336,0H.

Hendy YHM, Abdel Rahman HI. 2022. Photometric and statistical comparisons of the old open cluster M67 (NGC 2682) using KFISP and Gaia EDR3 astrometry. NRIAG J Astron Geophysics. 11(1):166–177. doi: 10.1080/20909977.2022.2040174.

Howell DC. 2002. Statistical methods for psychology. 5th ed. Pacific Grove (CA): Duxbury.

Landolt AU. 2013. UBVRI photometric standard stars around the sky at +50 deg declination. The Astronomical J. 146(5), p. 41. Article id. 131. doi: 10.1088/0004-6256/146/5/131.

Levene H. 1960. Robust tests for equality of variances. In: Olkin I Hotelling H, et al., editors. Contributions to probability and statistics: essays in honor of Harold Hotelling. Stanford University Press; p. 278–292.

Pandey AK, Nilakshi OK, Tarusawa R, Sagar K. 2001. VizieR online data catalog: UBVI photometry of NGC 7654 (M52. A&A. 374(2):504. doi: 10.1051/0004-6361:20010642.

Stetson PB. 1987. DAOPHOT: a computer program for crowded-field stellar photometry, publications of the astronomical society of the Pacific. Publications Of The Astronomical Soc Pac. 99:191. doi: 10.1086/131977.

Stetson PB, Diana M, Worrall CB, Barnes J. 1992. More experiments with DAOPHOT II and WF/PC images, astronomical data analysis software and systems I. A.S. P. Conference Series, Vol. 25. p. 297.